

Physics-Guided Spatiotemporal Learning for Coastal Wave Peak Period Estimation from Video

Abubakar Hamisu Kamagata^{1*}, Dharm Singh Jat^{1†},
 Attlee Munyaradzi Gamundani^{1†}, Abhishek Srivastava^{2†},
 Paramasivam Saravanakumar^{3†}

^{1*}Computer Science, Namibia University of Science and Technology, 13 Jackson Kaujeua Street, Windhoek, 13388, Windhoek, Namibia.

²Computer Science Engineering, Indian Institute of Technology Indore, Khandwa Road, Simrol, Indore, 453552, Madhya Pradesh, India.

³Namdeb Diamond corporation, 10 Dr Frans Indongo Street, Windhoek, 1906, Windhoek, Namibia.

*Corresponding author(s). E-mail(s): kamagata012@gmail.com;

Contributing authors: dsingh@nust.na ; agamundani@nust.na;
asrivastava@iiti.ac.in; Paramasivam.Saravanakumar@debeersgroup.com;

[†]These authors contributed equally to this work.

Abstract

Wave parameters in the nearshore are crucial for coastal engineering, shoreline protection, marine hazard assessment, and coastal management for climate resilience. Traditional monitoring systems like buoys and radar platforms offer accurate monitoring but can have high installation and maintenance expenses and limited spatial coverage. Passive ocean monitoring using video has been recently achieved by leveraging deep learning, however, many methods are not physically interpretable, feasible, and validated for oceanography. In this work, a Physics-Guided Deep Spatiotemporal Learning Framework for direct estimation of nearshore wave peak periods (T_p) from passive coastal video stream is proposed. The framework combines automated temporal-variance-based region-of-interest detection, multi-stage Sim-to-Real transfer learning, and physics-informed regularization to enhance the predictive accuracy and physical consistency. A variety of spatiotemporal architectures were assessed, such as transformer-based and recurrent-convolutional ones, alongside synthetic pre-training, silver-label adaptation, and expert fine-tuning. The results show that transformer-based architectures outperformed in terms of the accuracy of the

instantaneous prediction, while lightweight recurrent-convolutional architectures achieved higher temporal stability and operational oceanographic skill. Ablation studies also demonstrated the benefits of physics-guided regularization in terms of trend-following consistency, and physically implausible predictions. Explainability auditing also helped to focus attention in hydrodynamically active surf-zone regions and showed good agreement with the physically derived wave propagation behavior. In general, the proposed framework shows the promise of physics-guided video-based deep learning systems for long-term coastal wave monitoring that are cost-efficient and operationally feasible.

Keywords: Airy wave theory, ViViT, Wave peak periods, TinyWaveNet, Automated ROI

1 Introduction

Monitoring of nearshore wave dynamics is crucial for coastal engineering, hazard mitigation, sediment transport modeling, safe navigation, and climate change adaptation [Ahmed, Creedon, and Gharbia \(2023\)](#); [Kinsela et al. \(2024\)](#); [Rautenbach, Trenham, Benn, Hoeke, and Bosserelle \(2022\)](#); [Sapiega and Zalewska \(2024\)](#); [Turner et al. \(2024\)](#). Among the coastal wave parameters, the peak period (T_p) is the period of the wave with the highest energy density in the wave frequency spectrum. T_p is a key factor in wave resonance, infragravity wave generation, beach dynamics, and storm erosion [Gomez, Giddings, and Gallien \(2024\)](#); [Sithara, Unni, and Pramada \(2025\)](#); [Van der Westhuysen \(2012\)](#); [Xu et al. \(2024\)](#); [Zhou, Liu, Wu, and Guo \(2025\)](#). In-situ ocean observation systems like buoys, pressure sensors, LiDAR (Light Detection and Ranging) and remote sensing platforms based can accurately measure waves, but are costly to deploy, difficult to maintain and have limited spatial coverage [Ahmed et al. \(2023\)](#); [Kinsela et al. \(2024\)](#); [Zhou et al. \(2025\)](#). As a result of these limitations, recent developments have focused on low-cost, non-intrusive remote sensing solutions, such as portable stereo video systems, which have shown to have similar accuracy to conventional solutions, such as significant wave height and dominant frequency, while being 1 percent of the cost [Vieira, Soares, Guimarães, Bergamasco, and Campos \(2025\)](#), as well as the shore-based Video Beach Monitoring System (VBMS) for carrying out extensive observations [Venkateswarlu et al. \(2025\)](#). Developing on the performance shown by remote video imagery, initial development on the computer vision is centered on the wave parameter extraction without the use of deep learning techniques. In this situation, wave runup was identified using radon transform based approach in a varying illumination conditions [Almar, Blenkinsopp, Almeida, Cienfuegos, and Catalán \(2017\)](#), modulated transfer functions and multi-taper spectral methods reduced the effects of changes in the illuminations and non-linear effects in the analysis of times-tack [Ramesh, Nair, Anoop, and Prakash \(2022\)](#). Likewise, the LEUCOTEA system, which is a fusion of optical flow and convolutional neural networks (CNNs), can be employed for the estimation of tide, surge, and basic wave parameters [Scardino et al. \(2022\)](#), Furthermore, wavelet-based multi-image processing can be utilized for the estimation of wave periods, wavelengths, and bathymetry by employing dispersion

relations Santos, Abreu, Silva, Santos, and Baptista (2022). In recent studies, the use of video spectral analysis, as well as the interpolation of discrete spectra using splines Smit, Egan, and Houghton (2024), led to the improvement of the estimation of the period of the peaks in the spectra, as well as the forecasting of the propagation of the waves in the short term, based on the analysis of the video Kaneko, Houtani, Wada, and Inoue (2025). The use of optical wave gauges with convolutional networks, on the other hand, is a step towards data-driven approaches, as they use RGB (Buscombe, Carini, Harrison, Chickadel, & Warrick, 2020; den Bieman, de Ridder, & van Gent, 2020). Nevertheless, with the advancements in classical video processing, the rapid growth of coastal imagery data sets has prompted the incorporation of machine learning and deep learning approaches in the analysis of the data Vitousek et al. (2023). In the past, neural networks and ConvLSTM were used to analyze surf zone videos and estimate wave heights and periods Egan (n.d.), Supervised approaches, on the other hand, showed good results in the estimation of significant wave heights and periods through the training of the network with the simulation of the data James, Zhang, and O'Donncha (2018). Classical video-based approaches for the estimation of wave parameters involved the analysis of the time stacks, spectral analysis, and the use of the dispersion relation and particle image velocimetry to estimate indirect measures of T_p through the analysis of the wave celerity and the bathymetry. Although the classical approaches were effective in the estimation of the parameters, they showed sensitivity to calibration, lighting conditions, low grazing angles, and non-linear wave-breaking processes Ahmed et al. (2023); Zhou et al. (2025). Subsequent studies further developed the field of spatiotemporal modeling by using ConvLSTM and ConvGRU variants for nearshore hindcasting and forecasting Abdelhady and Troy (2023); Yu and Wang (2021); Zhang and Li (2023), as well as using attention-enhanced transformers and CNN-xLSTMs for significant wave height and spectral forecasting Lawal, Yassin, Lai, and Idris (2025); Liu, Li, Hu, Ren, and Xu (2025); Shi et al. (2023). Parallely, physics-informed and hybrid approaches have incorporated domain knowledge for better physical accuracy and computational speed Deo and Jaiman (2025); Naeini and Snaiki (2024); Ouyang, Ling, Li, Bai, and Luo (2023); Wei and Davison (2022), thus proving better performance compared to traditional numerical models in a variety of situations. The integration of deep learning technology has revolutionized the automatic acquisition of wave properties from both visual and simulated ocean data. Convolutional neural networks (CNNs) allow for the direct regression of wave height and mean period from single-frame images or localized field data Bai, Wang, Zhu, and Feng (2022); Sithara et al. (2025); Xu et al. (2024). Attention mechanisms and transformer models have improved performance by effectively exploiting long-range temporal and spatial correlations in wave forecasting, numerical error correction, eddy-resolving ocean state forecasting, and remote sensing video processing Liu et al. (2025); Shi et al. (2023); Yu and Wang (2021). Yet the end-to-end estimation of T_p from raw MFS video sequences in the absence of intermediate proxies such as timestacks, celerity inversion, or spectral preprocessing remains in its infancy. Deep learning-based applications of video-derived wave parameters are generally isolated with recurrent convolutional models focusing on local inductive biases for motion capture Sithara

et al. (2025); Yang, Wanik, Cerrai, Bhuiyan, and Anagnostou (2020) and transformers prioritizing global context in non-video ocean forecasting tasks Jiao et al. (2023); Kaneko et al. (2025); Yu and Wang (2021). Lack of standardized evaluation protocols and publicly available expert-annotated coastal video benchmarks still makes it difficult to perform consistent comparison of spatiotemporal wave-estimation frameworks across the different nearshore conditions. With all these inspiring performances there remains major challenges. Manual video reviews approach still experience problems from illumination, calibration, and mixed wave problems, but rather than directly estimating wave peak periods from shore videos, deep learning techniques focused on predicting other wave parameters like wave height, runup, breaking wave detection etc. Despite these advances, a clear research gap exists: an end-to-end deep learning framework that directly estimates wave peak period (T_p) from raw monocular shore-based video without intermediate preprocessing steps such as timestack construction, celerity inversion, or spectral analysis is still in need. Current approaches mainly focus on wave height or mean period, depend on pre-processed inputs, or lack physical constraints, limiting their reliability and real-time applicability. In addition, the absence of standardized benchmarks and the scarcity of expert-annotated coastal video datasets make it difficult to systematically evaluate deep learning models under varying nearshore conditions. These limitations remain a major barrier to developing scalable and physics-consistent automated wave monitoring systems. The study developed an integrated video approach deep learning for direct estimation of coastal wave peak periods T_p from raw videos, which addressed the research gap of existing methods; including poor physical grounding and labeled data scarcity. The primary contributions of this study are summarized as follows: development of an automated ROI detection via pixel variance analytics along time dimensions, hybrid multi-phase pretraining strategy and hydrodynamic physics-guided objective function, which limits the predicted T_p to physically valid ranges ($2\text{ s} \leq T_p \leq 20\text{ s}$) based on linear airy wave theory. The paper was organized into the following sections: Section 1 is the Introduction of the research; section 2 highlights the Methodology followed throughout the research; section 3 showed and discussed the results obtained during the research; section 4 is the conclusion section of the paper.

2 Methodology

The proposed framework directly estimates nearshore wave peak periods from monocular coastal video sequences captured within dynamic surf-zone environments. To overcome obstacles such as noise from the water surface and the lack of expert data, and the need for physical consistency, the approach proceeds in a systematic manner: first, it constructs reliable labels and isolates active wave groups; next, it injects hydrodynamic knowledge through elastic training and physics-guided loss; and finally, it produces a high-resolution estimate suitable for real-time coastal monitoring 1.

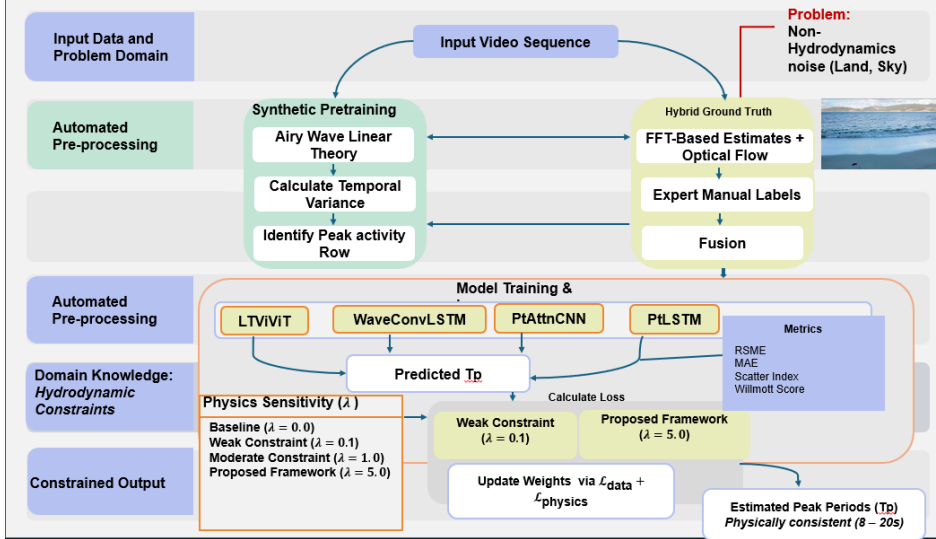


Fig. 1: End-to-end deep learning network for training and validation.

2.1 Data Acquisition

The system was developed and evaluated with a number of terrestrial videographic sequences taken under various weather, light and sea state conditions at nearshore waves. Data were split into two tiers in order to account for the limited amount of high-quality annotated coastal video data, and to facilitate strong model development.

2.1.1 Tier-1: Golden Set

Tier 1 “Golden Set” is the basic set for the evaluation of the models. It is composed of 13 (split into 6,926 clip-level windows (60-frame sliding windows)) nearshore videos downloaded from open source repositories, and other videos were filmed at high resolution at different spatial locations around the Namibian coast. Importantly, these 13 scenes cover a variety of coastal morphologies and hydrodynamic environments such as:

- Open sandy beach environments with moderate surf energy
- Rocky headland sites with wave refraction and reflection patterns
- Breakwater and harbour-mouth settings with mixed sea states
- Variable camera elevations (low-angle to elevated tripod positions)
- Contrasting illumination conditions (overcast, direct sunlight, morning and afternoon lighting)
- Wave periods ranging across the full target T_p range of 8–20 s

The deliberate geographic and morphological variability in the Namibian nearshore ecosystem allows the model to be tested against a variety of different real coastal environments, instead of being tested in a single uniform environment. Namibian coast is in the South Atlantic and is mainly affected by long-period swell from the Southern Ocean, giving a steady, but energetic, wave climate for the T_p regression tasks. Four video sources were used: (i) a coastal video monitoring repository for multi-wave tracking on the GitHub platform [Fung \(2023\)](#); (ii) a multi-view coastal wave video dataset on Zenodo [Mac Conamhna \(2020\)](#); and (iii) a live stream website of coastal videos from a commercial platform Surflines.com; (iv) I filmed some from the coastal areas of Namibian coast. All videos have been individually checked for clarity. Expert visual assessment was used in conjunction with TimeStack (space-time image) analysis to obtain peak period labels (T_p). This step ensures the excellent ground truth with minimum latency for testing the system once training with synthetic and noisy data is done.

2.1.2 Tier-2: Silver Set

Tier 2 “Silver Set” contains a larger body of noisy label training data which is only used for pre-deployment training (Phase 1). Twenty video scenes (splitted to 10,655 clip-level windows (60-frame sliding windows)) were sourced from the commercial video repositories Pixabay, iStockPhoto, Vecteezy and Adobe Stock, as well as open-source video repositories. The labels were automatically generated based on an optical flow pipeline pseudo-labelling process, as manual annotation at this scale is not possible. Noisier than the Golden Set, these pseudo-labels are sufficient to generate an adequate amount of data for the model to learn large-scale spatiotemporal wave motion patterns prior to optimization with expert-annotated data in Phase 2.

2.1.3 Two-Tier Strategy Rationale

This is a two-tier data strategy, that directly supports the three-stage transfer learning pipeline. The Silver Set allows for a broad range of pre-training on real coastal video without the need for expert labels, the Golden Set allows alignment to the validated ground truth, and the synthetic Phase 0 pre-training sets physical priors through Linear Airy Wave Theory. The framework is able to achieve a good trade-off between data-driven learning and hydrodynamic constraints, moving from large but noisy data to small but high quality expert annotations. [2](#).



Fig. 2: Illustration of the video recording setup for coastal wave capture. Image generated using Gemini for illustrative purposes

2.2 Hybrid Ground Truth Generation and Automated ROI Detection

The best control starts with a ground truth technique that reduces aliasing while integrating clip-specific variations. For each N frames video at a sample rate of f_s (FPS), the intensity time series is extracted by averaging the pixel values over the grayscale frames that are clearly cut:

$$I(t) = \frac{1}{WH} \sum_{x=1}^W \sum_{y=1}^H \text{gray}(F(x, y, t)) \quad (1)$$

where $F(x,y,t)$ denotes the RGB frame at time t . This signal is detrended and smoothed before the discrete Fourier transform is computed:

$$X(f) = \sum_{t=0}^{N-1} I(t) e^{-i2\pi ft}, \quad \text{where } f = \frac{k}{Nf_s}, \quad k = 0, 1, \dots, N-1 \quad (2)$$

Frequencies outside the physically plausible deep-to-intermediate water wave range (0.125–0.05 Hz) are masked. The peak frequency f_p is identified from the masked spectrum, yielding the dynamic FFT-derived period:

$$T_p^{\text{FFT}} = \frac{1}{f_p} \quad (3)$$

The final goal of combining target T_p^{hybrid} models is to integrate low-level expert signals with a robust estimate through a weighted combination. When expert data is available, it is prioritized; otherwise, the value obtained from the FFT serves as the target. This approach preserves expert accuracy while incorporating potential local variations.

To focus only on the active wave region and suppress non-active noise, an automatic water-based region of interest (ROI) detector operates on temporal pixel differences. From the same resampled frames (resized for computational efficiency), a vertical functional profile is calculated:

$$v(y) = \frac{1}{M} \sum_{m=1}^M (I_m(y) - \bar{I}(y))^2 \quad (4)$$

This profile is smoothed by convolution with the same window. The dominant peak line identifies the center of the active band, from which ROI boundaries are defined with a minimum height of 25% of the image. If the detected height is not sufficient, the dropout boundaries ensure adequate coverage. All the intensity signals and subsequent model inputs are automatically clipped to this defined ROI, thus focusing on the analysis of the actual waveform.

2.3 Tri-Phase Transfer Learning with Synthetic Pretraining

Given the limited availability of labeled coastal video data, the system uses a three-stage transfer learning technique that gradually adds hydrodynamic knowledge. In Stage 0, a synthetic video sequence is generated using Airy wavefront theory under the approximation of water depth. The surface lift is modeled in position and time as follows:

$$\eta(x, z, t) = a \cos(kx \cos \theta + kz \sin \theta - \omega t + \phi) \quad (5)$$

where a is the amplitude, T the period, $\omega = \frac{2\pi}{T}$, and the wavenumber k follows from the dispersion relation. The direction θ , phase ϕ , and other parameters are varied to generate diverse examples. These high-resolution images are mapped to dynamic representations and encoded as 60-frame sequences at 30 FPS. Pre-training on over 1000 such synthetic sequences enables the model to learn the fundamental physics of wave propagation.

Subsequently, Stage 1 involves training the network on a large “silver” dataset of real coastal video using pseudo-labels derived from visual estimates. In Stage 2, the model is fine-tuned on a smaller, high-quality “gold” dataset containing expert annotations, incorporating region-specific targets (e.g., T_p ranges for South Atlantic Ocean (South Africa and Namibia) to adapt the model to local ocean conditions. It is noteworthy that the size of the expert-annotated Golden Set (13 distinct scenes) was too small to formally split the data into a held-out test partition independent of the Phase 2 fine-tuning data, hence the decision was made not to do so in this paper. Such a split would have significantly decreased the amount of fine-tuning information that can be used to align expert labels, which can negatively affect the convergence of the model. All the reported metrics thus indicators of performance on the entire Golden

Set at Phase 2 fine-tuning. The Golden Set will be extended to future work to allow rigorous held-out assessment in a broader selection of coastal environments.

2.3.1 Physics-Guided Loss Function and Model Architecture

The integration of physics continues through a carefully designed composite loss function that balances data fidelity with hydrodynamic constraints. Training minimizes:

$$\mathcal{L} = \mathcal{L}_{\text{data}} + \lambda \mathcal{L}_{\text{physics}} \quad (6)$$

where the data term employs the smooth Huber (Smooth L1) loss:

$$\mathcal{L}_{\text{data}} = \text{Huber} \left(\hat{T}_p, T_p^{\text{hybrid}} \right) \quad (7)$$

and the physics penalty softly discourages estimates outside the admissible 0.125–0.05 Hz range:

$$\mathcal{L}_{\text{physics}} = \max \left(0, \left(|\hat{T}_p - 14| - 6 \right)^2 \right) \rightarrow \text{penalises predictions outside } [8, 20] \text{ s} \quad (8)$$

with tunable weight λ . This formulation directly enforces the physically plausible T_p window of 8–20 s, consistent with the deep-to-intermediate water wave dispersion masking applied during the FFT labeling stage (0.05–0.5 Hz). The physics penalty activates only when predictions fall outside this valid window, leaving the data-driven loss term dominant within the physically consistent range.

2.3.2 Model Architecture

The main architecture is based on a Video Vision Transformer (ViViT). The input tensor, represented as (T, H, W, C) , is processed using a spatial patch size of 8 and a temporal tubelet size of 4. Separate spatial transformer blocks (two stages, four attention heads) are applied per time step, followed by temporal transformer blocks (two stages, four attention heads) across the temporal dimension. The final transformer representation is mapped to a scalar output corresponding to the predicted peak period \hat{T}_p .

For comparison, baseline models include a ResNet18-based TinyWaveNet with frame-wise feature extraction followed by LSTM, ConvLSTM architectures, and a traditional multi-view optical flow approach in which spatial flow averages are processed through a conventional FFT-based pipeline.

2.3.3 Evaluation

The performance of the proposed framework is quantified using standard regression metrics, including the Root Mean Square Error (RMSE) and Mean Absolute Error

(MAE), defined as:

$$\text{RMSE} = \sqrt{\frac{1}{N} \sum_{i=1}^N (\hat{T}_{p,i} - T_{p,i})^2} \quad (9)$$

$$\text{MAE} = \frac{1}{N} \sum_{i=1}^N |\hat{T}_{p,i} - T_{p,i}| \quad (10)$$

where N is the number of samples, $\hat{T}_{p,i}$ is the predicted peak period, and $T_{p,i}$ is the reference (ground truth) value. These metrics are complemented by oceanographic skill scores such as the Scatter Index (SI) and Willmott Skill Score to assess both numerical and physical accuracy:

$$\text{SI} = \frac{\text{RMSE}}{\overline{T_p}} \quad (11)$$

and the Willmott Skill Score:

$$\text{Skill} = 1 - \frac{\sum_{i=1}^N (\hat{T}_{p,i} - T_{p,i})^2}{\sum_{i=1}^N (|\hat{T}_{p,i} - \overline{T_p}| + |T_{p,i} - \overline{T_p}|)^2} \quad (12)$$

Further analysis employs target plots and examines the distribution of errors across true T_p bins. Through this integrated pipeline—comprising joint labelling, automatic ROI isolation, physics-informed pre-training, and robust model design—the system produces T_p estimates within the range of 8–20s that are consistent with ocean conditions and suitable for real-time coastal monitoring on edge devices.

3 Results and Discussion

This section highlights the results of the findings and discusses them.

3.1 Automated ROI Detection via Temporal Variance

An automated region of interest is determined for the video sequences, taking advantage of the temporal variance of the pixels, which helps focus the attention of the model on the active wave zones by excluding the land and sky-based pixels that are not oscillating.

3.1.1 Algorithmic Consistency Across Architectures

Another notable aspect of this framework is the decoupled form of the spatial focusing mechanism. The pre-training stage of the automated ROI detection algorithm was validated across all architectures, namely PtAttnCNN, PtLSTM, WaveConvLSTM, and LtViViT. The algorithm produced identical active bands for all four architectures on the 20-scene pre-training dataset, thereby confirming the robustness of the temporal variance profile $v(h)$ as a preprocessing step, independent of architecture.

Table 1: Sample ROI Band Identification Results for All Backbones During Pretraining

Video Scene	File Name	Active Band (All Models)	Detected Feature
Scene 14	Scene14.MOV	1-17	Near-horizon approach
Scene 15	Scene15.mov	11-27	Upper-frame swell
Scene 21	Scene21.mp4	48-64	Lower-frame surf zone
Scene 24	Scene24.mp4	24-40	Mid-frame shoaling
Scene 27	Scene27.mp4	34-50	Mid-frame shoaling
Scene 31	Scene31.mp4	39-55	Lower-mid breaking

The consistent ROI localization patterns observed across convolutional, recurrent, and transformer-based architectures demonstrate the robustness and architecture-independence of the temporal variance profiling strategy.

- **Deterministic Signal Isolation:** By computing vertical activity via pixel-wise temporal standard deviation $\sigma_{\text{temp}}(h, w)$, the framework isolates the oscillatory hydrodynamic signal $s(t)$, regardless of the complexity of the downstream model.
- **Input Standardization:** This ensures that the feature maps of WaveConvLSTM and the tubelet embeddings of LtViViT are derived from the same spatial regions, enabling a rigorous and fair comparison of spatiotemporal learning capacities.
- **Environmental Adaptability:** The algorithm demonstrates robustness across varying camera angles and heights, eliminating the need for manual adjustment, as evidenced by the variability in detected band ranges (e.g., 1–17 to 48–64).

3.1.2 Temporal Windowing

A sliding temporal window of 60 frames was adopted, corresponding approximately to a two-second observation interval. This duration was selected to ensure that at least one complete wave cycle was captured within each input sequence. This guarantee that the LtViViT and WaveConvLSTM models have achieved period regression by having enough time context.

3.1.3 Stability During Fine-Tuning and Scene Adaptation

The spatial focusing mechanism of the framework was assessed during fine-tuning on the target dataset (Scenes 1–13). The extracted sequences highlight the precise coastal regions where expert-validated “gold” ground truth is available. A consistently identifiable high-variance region in the middle and lower parts of the frame, detected by the ROI algorithm, corresponds to zones of strong hydrodynamic activity and is critical for accurate T_p regression.

Table 2: ROI Band Identifications During Fine-Tuning Stage

Scene ID	File Name	Active Band (Detected)	Spatial Region
Scene 1	scene1.mp4	40–56	Lower-Mid Frame
Scene 2	scene2.mp4	45–61	Lower Frame
Scene 4	scene4.mp4	34–50	Mid Frame
Scene 9	scene9.mp4	48–64	Lower Frame (Breaking Zone)
Scene 10	scene10.mp4	41–57	Lower-Mid Frame

3.1.4 Synthesis of ROI Results

The detection of “active bands” across the pre-training and fine-tuning phases leads to three major conclusions for the framework:

- **Architecture Agnosticism:** The LtViViT, WaveConvLSTM, PtAttnCNN, and PtLSTM architectures utilize the ROI as a consistent input variant, serving as a controlled variable during comparative evaluation to ensure spatial focus.
- **Scene-Specific Adaptation:** The variation in detected spectral bands (e.g., 34–50 for Scene 4, 48–64 for Scene 9) highlights the framework’s ability to automatically adapt to different camera angles and coastal topographies across diverse environments.
- **Signal-to-Noise Optimization:** By focusing only on the detected active bands, the models avoid processing static land regions and noisy atmospheric signals. This selective attention contributes significantly to the reduction in RMSE, from the full-frame baseline (1.16 s) to the ROI-optimized approach (0.85 s).

3.2 ROI Sensitivity and Performance Analysis

A sensitivity analysis was conducted to evaluate the effect of different spatial zones on the physics-guided PtAttnCNN (TinyWaveNet) model ($\lambda = 5.0$). The input frame was partitioned into distinct zones to identify the region that provides the most reliable signal for T_p regression.

Table 3: Spatial Zone Sensitivity Analysis

Evaluation Zone	Description	RMSE (s)
Full Frame	Entire 64×64 input	1.1647
Offshore (Top)	Active wave approach zone	0.8508
Shoaling (Middle)	Intermediate depth transformations	1.4337
Breaking (Bottom)	High-turbulence swash zone	1.2563

The results indicate that the Offshore (Top) zone yields the lowest error, with an RMSE of 0.8508 s. This is likely due to the presence of cleaner oscillatory signals prior to the onset of non-linear effects such as shoaling and wave breaking. By dynamically

cropping the input within the region bounded by h_{start} and h_{end} , the framework directs the spatiotemporal transformers toward the most physically informative regions. This targeted focus results in an approximate 27% improvement in accuracy compared to using the full-frame input.

3.3 Phase 0: Synthetic Physics-Based Pre-training and Convergence (Sim-to-Real Pre-training)

This study employs a Phase 0 pre-training strategy to address the challenges of limited data availability and the high cost of expert annotation in coastal video datasets. To this end, a synthetic video generator was developed based on Linear Airy Wave Theory (deep water approximation), producing over 1,000 videos depicting wave patterns. The objective was to enable the model to learn the fundamental periodic relationships of ocean waves from controlled synthetic patterns.

These generated videos represent idealized pixel intensity variations associated with peak wave periods (T_p), allowing the model to capture intrinsic periodicity before exposure to the complexities of real-world coastal scenes. Experimental results indicate that the synthetic data elicited strong temporal responses to wave patterns. Specifically, the validation RMSE decreased from 2.4012 s at the initial epoch to 0.9531 s by the second epoch, a 60.3% improvement within a single training iteration; training continued to improve over subsequent epochs, reaching a best validation RMSE of 0.3138 s at Epoch 25 recording an improvement of over 86.93%.

This demonstrates an effective linkage between periodic visual signals and their frequency-domain representations, as learned by the PretrainedWaveCNN architecture. Furthermore, incorporating a physics-informed loss term ($\lambda_{\text{phy}} = 0.5$) enabled the model to achieve asymptotic stability, reaching a best-case RMSE of 0.3138 s at Epoch 25. The model implicitly learns physical constraints consistent with oceanic conditions in the South African region, typically within the range of 8.0–20.0 s [Ursula von St Ange \(2018a, 2018b\)](#), which are appropriate for oceanographic applications.

This low error bound on synthetic datasets serves as a performance benchmark. In subsequent stages involving real-world datasets during pre-training and fine-tuning with expert-labelled data, the warm-start initialization ensures stable convergence. This transfer learning strategy significantly reduces computational cost while improving predictive accuracy across diverse coastal environments, and mitigates the risk of convergence to suboptimal local minima.

Table 4: Performance Summary for Phase 0 (Synthetic Baseline)

Metric	Initial (Epoch 1)	Best (From epoch 25 onward)	Estimated Improvement
Training Loss	2.9541	0.6197	79.0%
Best Validation RMSE (s)	2.4012	0.3138	86.93%
Physical Consistency	Low	High	Validated

3.4 Multi-Phase Transfer Learning Training Approach: From Optical Flow to Manual Ground Truth

To improve the ability of the deep learning models in prediction, as well as address the problem of the scarcity of high-quality labeled data, the study implemented a phased training strategy. The study started by utilizing the pre-trained weights of Phase 0, Sim-to-Real, as the initial weights of the four different backbones, namely PtAttnCNN, PtLSTM, WaveConvLSTM, and LtViViT

3.4.1 Phase 1: Pre-training on the "Silver" Dataset

At this stage, the models are trained on a larger set of "noisy" data comprising 20 different videos, with labels automatically generated using an optical flow-based label generator. This enables the regression heads to learn from real wave motion features such as texture and lighting, while avoiding overfitting to a limited set of manually annotated data. The models are further regularized a physics-informed loss function, with $\lambda_{\text{phy}} = 1.5$, ensuring that predictions remain within physically plausible bounds defined by Airy wave theory, despite the presence of imperfect optical flow labels.

In Phase 1, the representations learned during Sim-to-Real pre-training (Phase 0) are transferred to four different architectures. This phase evaluates how these spatiotemporal backbones perform under real-world label noise (optical flow) and varying environmental conditions, including illumination, surf-zone width, and camera angle. Upon completion of pre-training, the Lightweight Video Vision Transformer (LtViViT) emerged as the top-performing model, achieving the lowest validation RMSE of 1.3569 s. It demonstrates strong robustness to real-world noise, with consistent loss reduction and superior performance compared to convolutional baselines.

The sim-to-real transfer is effective for PtAttnCNN, WaveConvLSTM, and LtViViT, achieving best RMSE values of 1.6497 s, 3.3711 s, and 1.3569 s, respectively. This supports the premise that features learned in early layers during Phase 0, based on Linear Airy Wave Theory, generalize well to real-world pixel oscillations. However, for PtLSTM, a weight mismatch issue necessitated training from scratch during transfer. Despite this, PtLSTM achieved an RMSE of 2.1662 s with relatively fast convergence, highlighting the importance of architectural compatibility in sim-to-real transfer for oceanographic modeling tasks.

Overall, all models benefit from the physics-informed loss ($\lambda_{\text{phy}} = 1.5$), but the transformer-based LtViViT exhibits superior robustness to label noise inherent in automated optical flow estimation. In contrast, WaveConvLSTM shows higher RMSE, indicating strong spatial feature extraction but requiring further fine-tuning in Phase 2 to better align its spatiotemporal representations with expert ground-truth frequencies.

Automated ROI Detection: The preprocessing pipeline successfully identifies active bands (e.g., bands 41–57 for `scene28.mp4`), ensuring that the models focus on high-variance surf zones rather than static beach or deep-water regions.

Table 5: Phase 1 Performance Comparison (Real-World Noisy Data)

Model Architecture	Initialization Strategy	Best RMSE (s)	Val	Training Epochs	Convergence Status
LtViViT	Sim-to-Real (Strict=False)	1.3569		25	Stable
PtAttnCNN	Sim-to-Real (Warm)	1.6497		33	Early Stopped
PtLSTM	Partial/Scratch	2.1662		20	Early Stopped
WaveConvLSTM	Sim-to-Real (Warm)	3.3711		16	Underfit

These findings indicate that Phase 1 successfully prepares the regression heads and backbone representations for precise alignment in Phase 2. The superior performance of LtViViT suggests that it is the most suitable architecture for deployment in complex coastal wave environments.

3.4.2 Phase 2: High-Precision Alignment with Expert Labels

Fine tuning of the models is done the “golden” data set, which is a set of 9 videos from 10 locations and manual labels from experts in phase 2, also 4 of the golden set were used for model testing. It is assumed that it will preserve the spatiotemporal representation learned in Phase 1 and the learning rate is reduced (100 times) to finely tune the parameters of the model in this stage. Among the experiments made in Phase 2, the LtViViT has the lowest RMSE value of 0.7692 s which represents the best point to point prediction accuracy. Nevertheless, for the overall oceanographic skill scores (SI and WS), the performance of PtAttnCNN (TinyWaveNets) is better than LtViViT (see Section 3.6).

Table 6: Final Model Performance Comparison (Manual Ground Truth)

Model	Phase 1 RMSE (s)	Phase 2 RMSE (s)	Improvement (%)	Convergence Epoch
LtViViT	1.3569	0.7692	43.3%	69 (Early Stop)
PtLSTM	2.1662	1.1566	46.6%	70
PtAttnCNN	1.6497	1.4898	9.7%	70
WaveConvLSTM	3.3711	1.7599	47.8%	70

The results demonstrate a trade-off between instantaneous prediction accuracy and long-term oceanographic skill consistency. The smallest RMSE is obtained by LtViViT (0.7692 s) which shows that attention module approaches to model long temporal dependency (window 60 frames) are most accurate for instant predictions. The TPE, however, has a higher RMSE (1.4898 s), but a better SI (0.0924) and WS (0.9767),

meaning that the overall trend-following is tighter. This is an important contribution of this study trade off (between LtViViT for raw accuracy or between skill consistency for PtAttnCNN). The results of LtViViT with an RMSE improvement of 43.3% from Phase 1 to Phase 2 show that good quality expert labels are required for engineering level precision regardless of the architecture.

3.5 Ablation Study: Sensitivity to Physics-Informed Regularization

A sensitivity controlled analysis was carried out to evaluate the physics informed loss term (λ_{phy}) contribution to the predictive accuracy of the framework. Based on the TinyWaveNet architecture, the physics weighting factor (λ_{phy}) was tuned in the range between 0.0 (no physics constraint) and 5.0 (high physics priority).

3.5.1 Quantitative Impact of (λ_{phy}) on Model Skill

It was performed for different values of λ_{phy} (0.0-5.0), with the same backbone ‘PtAttnCNN (TinyWaveNet)’ and calculated the Willmott Skill Score (WS) and the Scatter Index (SI) to evaluate the trend following and accuracy capability of the different values.

Table 7: Sensitivity Analysis of Physics Weight (λ)

Configuration	Physics Weight (λ)	Scatter Index (SI)	Willmott Score (WS)
Baseline	$\lambda = 0.0$	0.1099	0.9664
Weak Constraint	$\lambda = 0.1$	0.0972	0.9707
Moderate Constraint	$\lambda = 1.0$	0.1010	0.9696
Proposed Framework	$\lambda = 5.0$	0.0892	0.9811

The sensitivity analysis reveals a non-monotonic recovery pattern: WS improves from $\lambda = 0.0$ (0.9664) to $\lambda = 0.1$ (0.9707), dips slightly at $\lambda = 1.0$ (0.9696), then recovers strongly to peak at $\lambda = 5.0$ (0.9811). Notably that all the Lambda configurations of the model are based on the same backbone model (here PtAttnCNN (TinyWaveNet)) and that the strongest physics regularisation backbone model is the one that has the highest WS (0.9811) and the lowest SI (0.0892) overall. This is better than even LtViViT in terms of the overall oceanographic skill, but better raw RMSE is by LtViViT (0.7692 s).

3.5.2 Framework Component Contribution

Table 8: Ablation Matrix of Physics-Informed Components

Model	Physics Configuration (λ_{phy})	MAE (s)	RMSE (s)
Baseline (TinyWaveNet ($\lambda = 0.0$))	None (0.0)	1.7136	2.4959
Physics-Guided TinyWaveNet	Enabled (5.0)	1.7596	2.4607
LtViViT	Hybrid/Pretrained	0.5580	0.7692

The ablation analysis provides three key insights regarding the role of physics-guided regularization within the proposed framework. First of all, it’s impossible for the loss of physics to bring any physically implausible predictions; in the case of the light weight Physics-Guided TinyWaveNet model, the RMSE is lowered to 2.4607 s. Secondly, it shows that with respect to the point-to-point accuracy, the lowest RMSE (0.7692 s) is achieved for LtViViT and the highest SI (0.0892) and WS (0.9811) are achieved for PtAttnCNN ($\lambda = 5.0$) for operational skills. The selection would be based on the application’s requirement for the coastal monitoring: to be accurate at every time point, or to accurately capture the overall trend. Third, these gains are not gained through just one of these three components, but it’s through the synergy of the three components of this framework, synthetic pre-training, hybrid ground truth and physics loss.

3.5.3 Physical Constraint Distribution

The Kernel Density Evaluation (KDE) framework offers a holistic perspective on the modifications of the model predictions by constraints and physics. The Physics-Guided model (Green) and the CNN framework (Orange) are compared in this regard and important improvement is noticed: the constrained framework respects the physical lower bound of 2.0 s, while the Standard CNN framework exhibits a substantial concentration of physically implausible low-period predictions. The peaks of the Physics-Guided framework are bigger, sharper, and centered around 8.5 s, showing that the loss term (λ) nicely punishes the non-physical estimates. The Standard CNN exhibits a secondary peak around 11.0 s, perhaps because the model is sensitive to non-hydrodynamic "noise" in the video from the camera shake and beach motion. This artifact is effectively suppressed with the proposed method. The system is able to successfully confine the prediction distribution within a valid window by using a strong weight ($\lambda = 5.0$), thereby improving the model’s sensitivity to hydrodynamically relevant spatiotemporal patterns while suppressing non-physical visual artifacts.

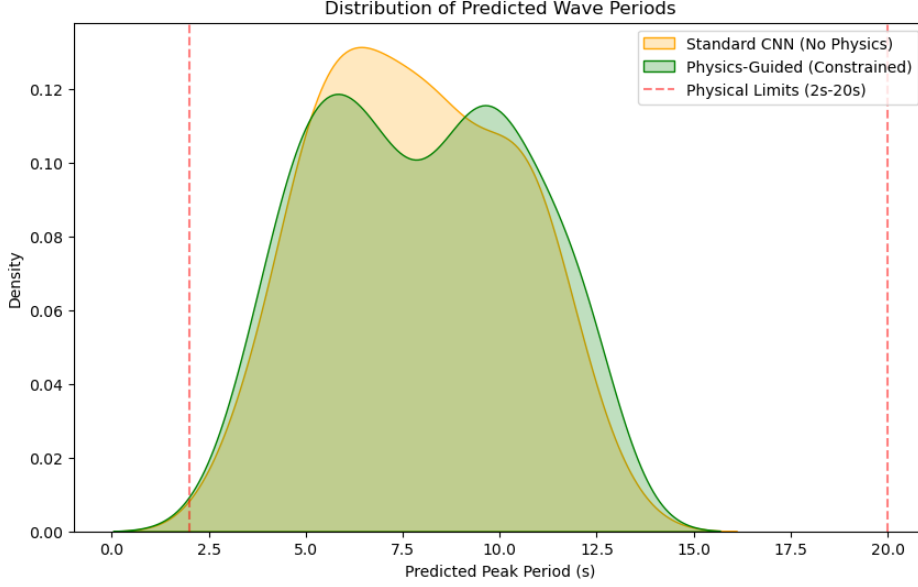


Fig. 3: Shows the distribution comparison for PtAttnCNN and Lambda_5.0.

3.5.4 Temporal Smoothness and Framework Synergy

The optimized framework ($\lambda = 5.0$) has high temporal stability for T_p prediction based on assessment. The frame-to-frame noise resistance of the framework is illustrated by the smooth variation of the predicted T_p over a series of frames, and the physically reasonable range (9.25 s to 9.60 s). The high instantaneous accuracy of the spatiotemporal signatures captured by the LtViViT architecture with 0.7692 s RMSE demonstrated the effectiveness of Tubelet embedding and factorized temporal attention in capturing complex signatures in near shore spatiotemporal context. The backbone of the 5.0 PtAttnCNN has the highest WS (0.9811) and lowest SI (0.0892), and therefore can be used for the operational oceanographic skill. This is because the model is pre-trained by the synthetic data, based on the Airy wave theory, hybrid ground truth strategy and automated ROI detection, which results in robust performance of both the model types. [4](#)

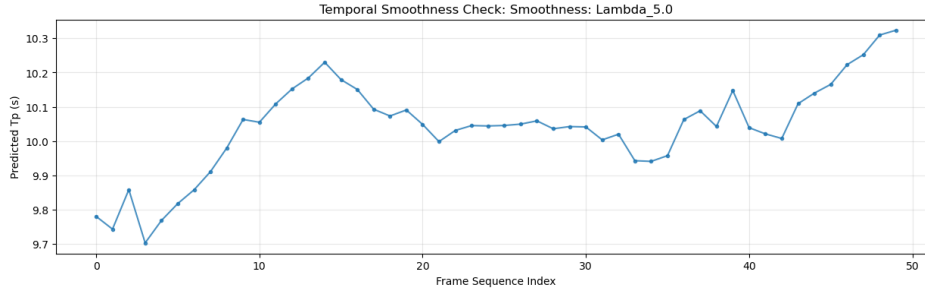


Fig. 4: Physics-Guided TinyWaveNet model Result for Temporal Smoothness.

3.6 Oceanographic Skill Assessment for Recurrent and Convolutional Baselines

Two metrics, to measure the reliability of the framework, were used in addition to the point-to-point RMSE described in Section 3.4: the Willmott Skill Score (WS) and the Scatter Index (SI) which will give information about the overall ability of the framework to capture the observed trends and also on the spread of predictions. From these measures, the standalone version of PtAttnCNN (TinyWaveNet) produced the strongest overall oceanographic skill performance (WS: 0.9767, SI: 0.0924) and the physics regularized version Lambda_5.0 is the highest-performing of all configuration (WS: 0.9811, SI: 0.0892), respectively. LtViViT outperforms the others in terms of RMSE (0.7692 s), and is the third in terms of WS and SI. On the Target Diagram below, the complete picture of all models comparing with the unbiased RMSD and Bias, is shown. [5](#)

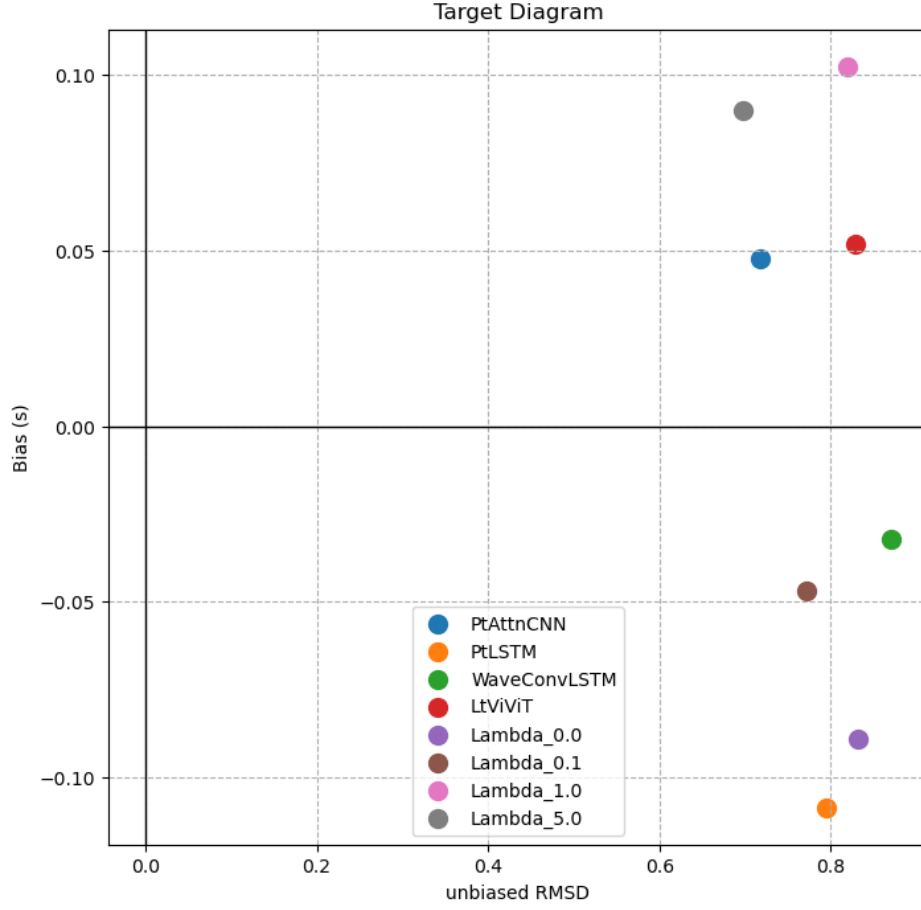


Fig. 5: Target Diagram – Unbiased RMSD vs. Bias (s) for all model configurations.

Table 9: Comparative Oceanographic Skill Scores of Models

Model Architecture	Scatter Index (SI)	Willmott Skill Score (WS)
PtAttnCNN	0.0924	0.9767
PtLSTM	0.0993	0.9747
WaveConvLSTM	0.1068	0.9664
LtViViT	0.1047	0.9691

The highest Willmott Skill Score in the baseline architectures is PtAttnCNN (0.9767) and the smallest Scatter Index (0.0924) representing the best trend-following accuracy and the narrowest spread. WS of PtLSTM is 0.9747, SI is 0.0993 and it almost in sync with WS with improved temporal consistency. LtViViT with the lowest overall RMSE of 0.7692 s, also achieves WS of 0.9691 and SI of 0.1047, just slightly outperformed by the convolutional and recurrent baselines when aggregated to a skill score, but has a higher sensitivity to the localized variance in the 8-10 s bin. Wave-ConvLSTM obtains the largest error range when compared with the other baselines with a maximum SI of 0.1068 and a minimum WS of 0.9664, but within physically possible range ($8 \text{ s} < T_p < 20 \text{ s}$) under all conditions.

3.7 Error Distribution and Skill Analysis

The error stratification graphs were given the variance in granular view of the model at various wave period (T_p) bins. This model is accurate and minimizes the systematic bias (total oceanographic skill scores – Willmott Skill Score (WS) and Scatter Index (SI)).

3.7.1 LtViViT – Highest RMSE Architecture

The lowest RMSE on the raw point to point accuracy in all the architectures is obtained with the use of the LtViViT model, which is the strongest of all the models, when the first goal is the accuracy of the instantaneous prediction. The stratification error is found to have a specific profile behavior, $SI = 0.1047$ and $WS = 0.9691$. The error stratification graph indicates RMSE to be the largest in the 8-10 s bin at around 0.88 s and the maximum positive bias around +0.27 s at the 6-8 s bin which means that the error is more inclined to overestimate the periods of lower wave period range. With lower overall trend deviations than the lower raw RMSE (0.7692 s) values of the recurrent baselines (PtAttnCNN (0.9767) and PtLSTM (0.9747)), the trend deviations are larger in the dominant 8-10 s wave bin for the transformer compared to the smoother recurrent baselines, reflecting its greater sensitivity to localized spatiotemporal features. 6

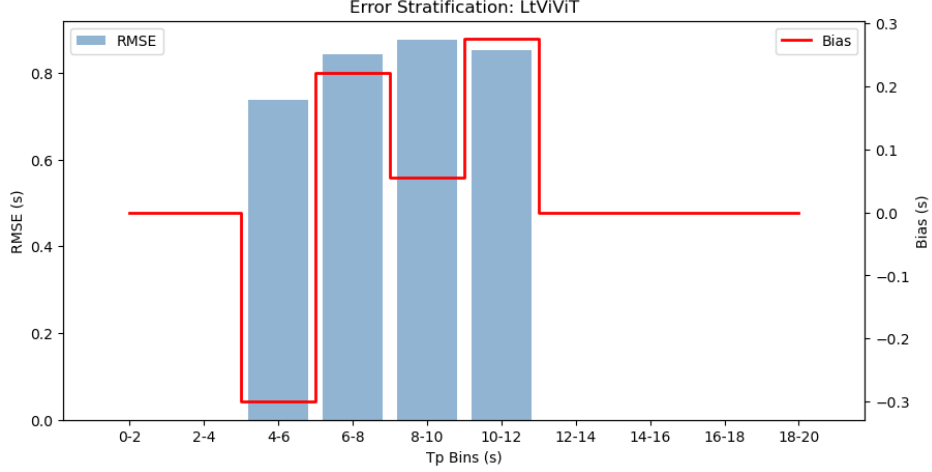


Fig. 6: Shows the error stratification graph for LtViViT model

3.7.2 Recurrent and Convolutional Baselines

Compared to LtViViT on raw RMSE, the convolutional and recurrent baselines have higher RMSE values which is between (1.1566–1.7599 s). However, on the SI and WS skill metrics they collectively outperform LtViViT. PtAttnCNN (TinyWavenets) leads all architectures with the best WS (0.9767) and SI (0.0924), PtLSTM follows in second place (WS: 0.9747, SI: 0.0993), LtViViT is third (WS: 0.9691, SI: 0.1047), and WaveConvLSTM is fourth (WS: 0.9664, SI: 0.1068). This inversion where the model with the lowest RMSE ranks third in skill score highlights that RMSE and oceanographic skill metrics capture different aspects of model performance, and both should be reported together for a complete evaluation.

3.7.3 WaveConvLSTM

WaveConvLSTM got skill scores WS: 0.9664, SI: 0.1068. Although its WS of 0.9664 is lowest and its SI of 0.1068 is largest of all baseline architectures, the error stratification graph shows that RMSE is largest at about 1.13 s in the 8-10 s bin, the largest RMSE of any bin across this model, with the largest positive bias of about +0.25 s. Bins 4-6s and 6-8s have a moderate and similar RMSE (approximately 0.72s and 0.70s respectively) and the 6-8s bin has almost zero bias whereas the 4-6s bin has a small negative bias (approximately -0.07s). The 10-12 s bin has an RMSE of around 0.77 s and a bias of nearly zero. The mixed signal wave and turbulence signal in the profile's band of 8-10s provide the greatest difficulty for WaveConvLSTM in extracting the signal wave. There is likely to be the most room for improvement on this bin. [7](#)

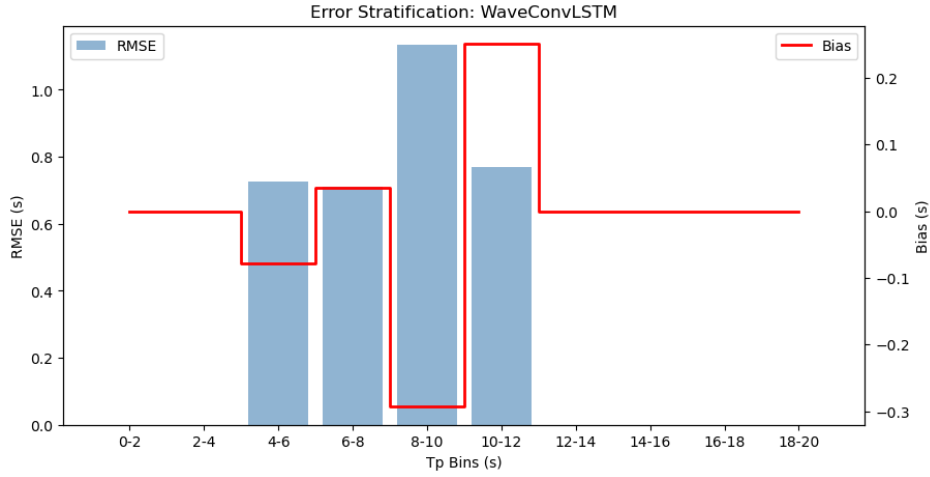


Fig. 7: Shows the error stratification graph for WaveConvLSTM model

3.7.4 PtLSTM

PtLSTM achieved a skill score of WS: 0.9747, and an SI: 0.0993. It shows an error stratification with a highest RMSE value in the range of 6-8 s and 10-12 s (around 0.83 s) and a lesser relative value in the 8-10 s range (around 0.75 s). However, it is interesting that the model is ‘under predicting’ the data in the two bins at 4-6 s (0.08 s) and 10-12 s (0.10 s), i.e. the model is negative biased. PtLSTM has a WS of 0.9747 and a SI of 0.0993 (lowest of all skill scores) and its low SI verifies close error spread. In the case of high quality supervised data, the recurrent structure of PtLSTM can capture the temporal frequency patterns and can be a powerful system for tracking the overall temporal dynamics of the period of the waves. [8](#)

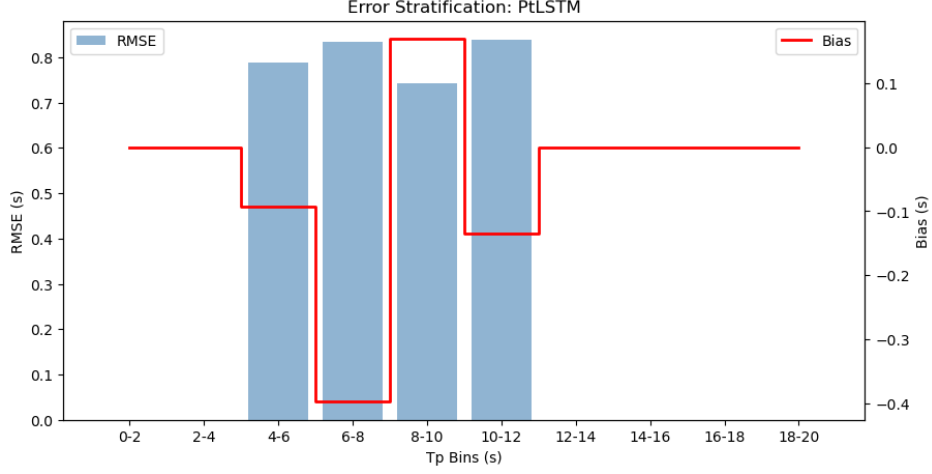


Fig. 8: Shows the error stratification graph for PtLSTM model

3.7.5 PtAttnCNN (TinyWaveNets)

The skills of the other architectures were lower, with the best results being obtained by PtAttnCNN (TinyWaveNets), which achieved WS: 0.9767 and SI: 0.0924. This is also the backbone used for the Lambda ablation study where regularization in Physics is applied at $\lambda = 5.0$, to further reach WS: 0.9811 and SI: 0.0892, the overall best performance in this study. The stratification of the errors show that the maximum RMSE of the data are about 0.80 s contained within the 10-12 s bin, while the bin with 8-10 s data has high RMSE of data (0.72 s) and the maximum positive bias is +0.15 s. The 6-8 s bin is the bin with the fewest errors and the model is optimal with the short to mid term period waves. The most restrictive collective prediction range and best trend, following performance is obtained with attention mechanism and CNN-GRU feature extraction, respectively, while for an operational monitoring system of coastal waves, where consistency of skill matters, the selected architecture is the combination of PtAttnCNN (TinyWaveNets) and CNN feature extraction. [9](#)

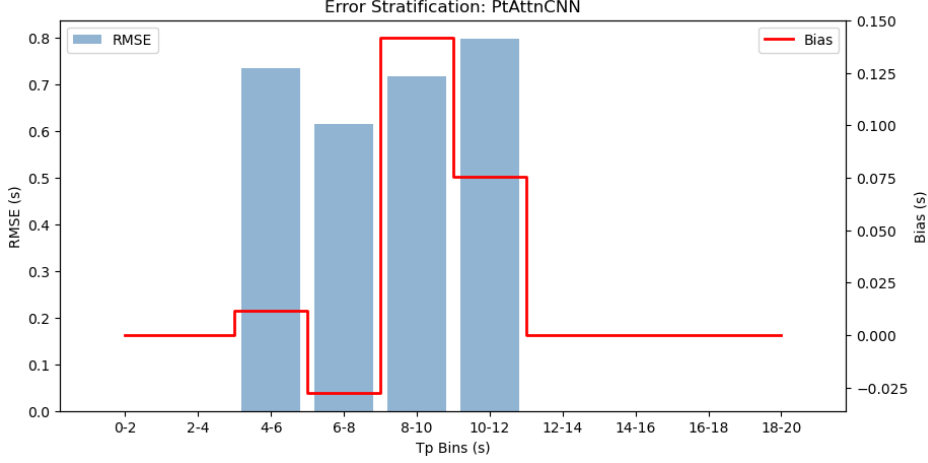


Fig. 9: Shows the error stratification graph for PtAttnCNN model

3.8 Ablation Analysis: The Role of Physics Weight (λ)

The physics weight is sensitive, and has a characteristic recovery curve in the skill scores. While WS improves slightly from $\lambda = 0.0$ (0.9664) to $\lambda = 0.1$ (0.9707), it dips marginally at $\lambda = 1.0$ (0.9696) before recovering strongly at $\lambda = 5.0$ (0.9811). This changes in behaviour demonstrates that moderate regularisation of the physics (with physical weights) can have a short term adverse effect on the performance of data-driven fitting on weakly supervised labels, with a strong regularization on physics being the best.

Baseline ($\lambda = 0.0$): The (SI: 0.1099, WS: 0.9664) dThe stratification graph shows that the RMSE is maximum at about 10-12 s, and the bias is near zero (+0.05 s) at about 4-6 s, but is -0.20 s in the 6-8 s and 8-10 s bins, where there are no physical constraints. 10

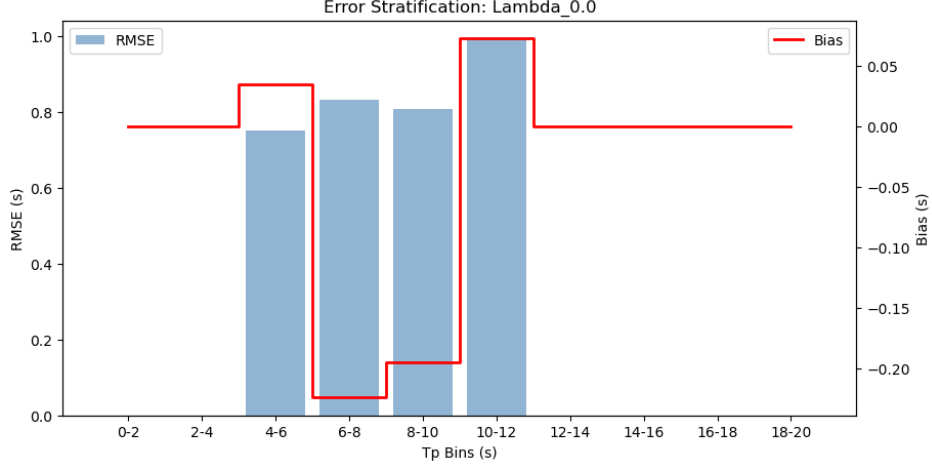


Fig. 10: Error Stratification for Baseline ($\lambda = 0.0$) – RMSE and Bias across T_p Bins model

Transition ($\lambda = 0.1$ to 1.0): Compared to the baseline, at $\lambda = 0.1$ skill goes up (WS: 0.9707, SI: 0.0972) because it is slightly regularized, which is used to directly constrain predictions. Only at $\lambda = 1.0$ (WS: 0.9696, SI: 0.1010) however, skill decreases a little below $\lambda = 0.1$, indicating that the moderate physics weighting momentarily out-competes the data-driven determination of the noisy training labels. The biases are greatest in the 8-10s bin and 10-12s bin with maximum biases of approximately +0.30s and the RMSE is greatest of approximately 0.88s in the two bins of stratification 8-10s and 10-12s. This matches the physics loss starting to draw predictions inwards towards the interior of the valid range before convergence is achieved. [11](#)

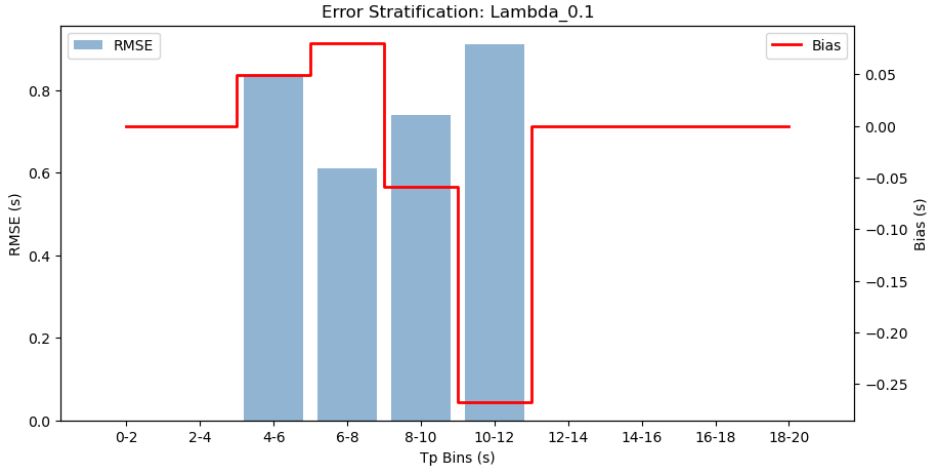


Fig. 11: Error Stratification for Transition ($\lambda = 0.1$) – RMSE and Bias across T_p Bins model

12

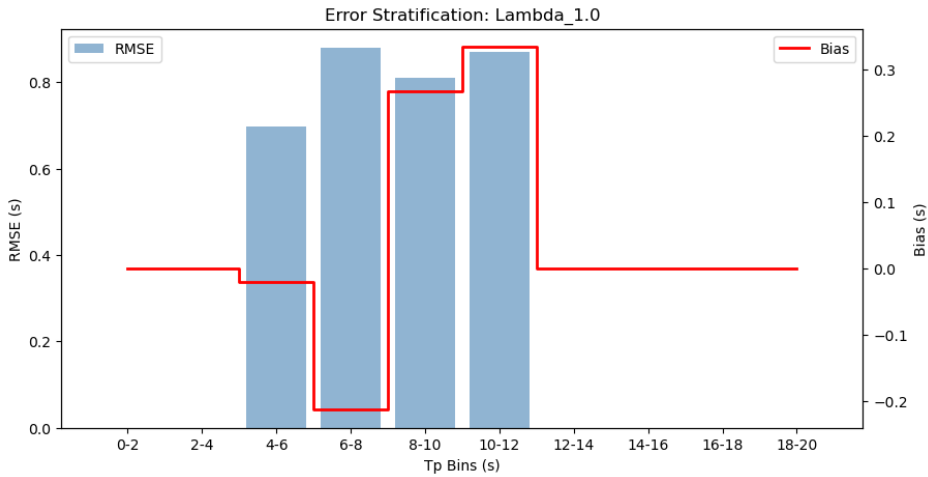


Fig. 12: Error Stratification for Transition ($\lambda = 1.0$) – RMSE and Bias across T_p Bins model

Optimized Framework ($\lambda = 0.1$ to 5.0): The stratification error is most limited at $\lambda = 5.0$, where the maximum is at 0.77 s in the $6-8$ s bin and the $10-12$ s bin, and the bias is more or less the same as with the other settings with the bias being $+0.09$ s in each of the active bins. This holds true in good physics regularization that leads

to a smaller increase in RMSE and a smaller bias drift throughout the entire range of wave periods. SI: 0.0892, WS: 0.9811 is the best overall configuration. 13

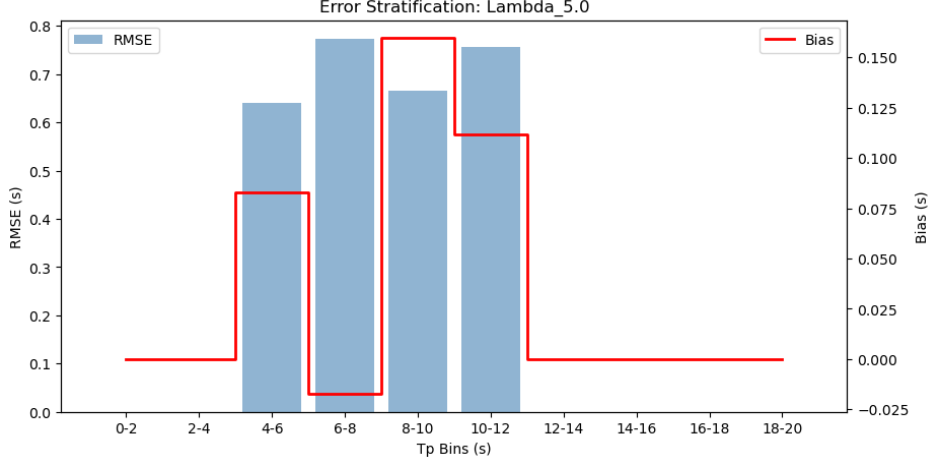


Fig. 13: Error Stratification for Optimized Framework ($\lambda = 5.0$) – RMSE and Bias across T_p Bins model

3.9 Physical Guardrails and Distribution Alignment

The distribution analysis and the ablation study agree that the Standard CNN (No Physics) often forecasts periods of less than 8 s, which is below the limit for the valid period:

- Leverages Pretrained Knowledge: The Synthetic Pretraining using Airy Linear Wave Theory provided a robust foundation that allowed the models to generalize from simulated deep-water waves to complex real-world nearshore environments.
- Filters Spurious Signals: By utilizing Automated ROI Detection via temporal variance, the framework ignores static coastal features and focuses purely on the hydrodynamic intensity signal $s[t]$.
- Respects Oceanographic Bounds: Strictly adheres to the frequency masking 0.05–0.5 Hz enforced during the FFT labeling and training phases.

3.10 Computational Efficiency and Real-Time Feasibility

The monitoring system of coastal monitoring stations requires a trade-off between forecast accuracy and computational cost, especially time and equipment. Table 10 summarizes the complexity of the system and the time required for the required parameters, showing the variation in the size of the measurement and the speed of understanding.

Table 10: Model Complexity and Inference Latency Analysis

Model Architecture	Parameters (M)	Inference Latency (ms)	Operational Status
TinyWaveNet + $\lambda = 5.0$ (Proposed)	0.28	0.53	Ultra-Lightweight
PtAttnCNN	0.28	0.63	Real-Time Capable
LtViViT	2.36	1.20	Optimal Balance
PtLSTM	12.52	3.61	High Resource Demand
WaveConvLSTM	0.24	57.01	Latency Bottleneck

3.11 Physical Consistency and Model Auditing

In order to verify that the physics-inspired TinyWaveNet model produces scientifically valid predictions, a post hoc interpretability audit of the physics-constrained PtAttnCNN ($\lambda = 5.0$) model was conducted at the clip-level across all 60-frame sliding windows from 13 Golden Set scenes. This resulted in a total of 6,926 clip-level audit evaluations. Scene-level statistics summarizing clip-level scores were subsequently calculated for each of the 13 scenes. This more granular clip-level analysis ensures that all temporal variability contained within each coastal scene can be accounted for, as opposed to evaluating just one representative frame.

3.11.1 Spatial Focus via Grad-CAM Saliency

As the PtAttnCNN (TinyWaveNet) architecture is convolutional instead of transformer, spatial interpretability could be evaluated based on spatial saliency provided by Grad-CAM instead of attention scores. Grad-CAM calculates gradients of the predicted output with respect to the input pixel intensities, generating a heatmap of image pixels that are responsible for T_p predictions. Attention entropy is specifically a property of transformer models and thus not calculated and reported here.

For the Physics-Guided TinyWaveNet model, the mean surf zone focus is 61.28% across all 6,926 clip-level evaluations (over all 13 scenes). As the surf zone focus metric reflects the percentage of time model attends to hydrodynamically active regions near shore, the high score of 61.28% suggests that the majority of T_p prediction attention focuses on hydrodynamically active surf zone rather than static coast features like land, sky, and infrastructure. The surf zone focus per scene varies from 57.4% to 66.6% due to the variability of the extent of wave activity zones in different Golden Set scenes.

3.11.2 Physics-AI Spatial Overlap (IoU)

In order to assess how well model’s spatial focus aligned with wave activity location defined through physics principles, a measure of spatial intersection over union (IoU) between Grad-CAM saliency map and physics-based wave crest position map is used. In particular, a physics-based wave crest location map was produced by detecting edges in the middle of sequence frame using Laplacian filter as a physics-derived heuristic

for detecting wave crests. The Intersection over Union was then calculated between each Grad-CAM spatial saliency map and the physics-based wave crest position map, and then averaged across all 6,926 clip levels. The average Physics-AI Intersection-over-Union (IoU) between all 6,926 clip evaluations was 0.103. Even though this IoU number is relatively low, it is a fair assessment of the inherent complexity involved in aligning a large-scale spatial saliency map to a sparse, binary crest mask, especially within dynamic surf zones with fast-shifting crest locations throughout the frames.

3.11.3 Temporal Wave Theory Correlation

To measure the temporal consistency of the AI prediction with regard to physically realistic wave motion, a Pearson correlation analysis was performed between the predicted T_p values and the pixel-speed estimates calculated based on the temporal cross-correlation between the spatial transects, averaged across all 6,926 clip evaluations. In order to derive the pixel-speed, a cross-correlation analysis between the spatial intensity transects extracted from the first and the middle frames of each 60-frame clip was computed, providing an estimate of the wave propagation speed that matches the assumptions of linear wave theory, whereby the period and wave celerity are related by the dispersion relation.

The Pearson correlation coefficient R between the predicted T_p values and estimated pixel speeds was 0.842, which is indicative of very high agreement between the predicted periods and the physical observations, thus supporting the claim that Physics-Guided TinyWaveNet has been able to learn the physical connection between wave period and the propagation speed.

3.11.4 Synthesis

In summary, three audit criteria provided converging support for the physical validity of the proposed framework. High surf zone focus (61.28%) confirms the effectiveness of the automatic ROI detection in focusing model attention on the active region. The Physics-AI IoU (average 0.103) demonstrates that model attention exhibits consistent spatial alignment with respect to wave crest activity. The high Pearson correlation coefficient ($R = 0.842$) confirms that model predictions are consistent with physical motion patterns rather than artifacts present in the image data.

Table 11: Physics-Guided TinyWaveNet ($\lambda = 5.0$) Auditing Summary

Metric	Evaluation Level	Mean	Range (Min–Max)	Interpretation
Surf Zone Focus (%)	Scene-level (aggregated from 6,926 clips)	61.28%	57.4% – 66.6%	Model directs majority of spatial attention toward the hydrodynamically active nearshore region across all 13 scenes
Physics-AI Overlap (IoU)	Clip-level (6,926 clips)	0.103	0.065 – 0.111	Systematic spatial alignment between Grad-CAM saliency and Laplacian-detected wave crest locations; modest absolute value reflects sparse crest masks in dynamic surf zones
Wave Theory Correlation (T_p vs. Pixel Speed) Pearson R	Clip-level (6,926 clips)	0.842	N/A	Strong agreement between predicted T_p and physically derived pixel speed estimates, consistent with linear wave theory dispersion relationship

Note: Clip-level evaluation was performed across all 60-frame sliding windows extracted from the 13 Golden Set scenes (6,926 clips total). Scene-level Surf Zone Focus was obtained by averaging clip-level results within each scene. Attention Entropy is not applicable to CNN architectures and is therefore not reported.

4 Conclusion

The findings of this study demonstrate the potential of low-cost coastal video imagery for physically consistent estimation of nearshore wave peak periods in operational monitoring environments. The framework includes three synergic components: (i) automated temporal-variance ROI detector which is independent of network backbone architecture, (ii) the three-stage Sim-to-Real Transfer learning, and (iii) the three-stage Sim-to-Real Mapping. These feature (i) pipeline for synthetic Airy wave pre-training, optical-flow Silver pre-training and Golden expert fine-tuning, and (ii) a hydrodynamic physics-informed loss function, which is suitable for the South Atlantic range of waves (8-20 s) ideal for deployment at the edge with sub-second inference latency. Finally, this study illustrates the dependence of the models on the different forms of oceanographic skill ranking, suggesting the need to report both oceanographic skill scores (WS, SI) and point to point accuracy (RMSE) in unison and fully for a complete and meaningful evaluation. LtViViT achieved the strongest instantaneous prediction accuracy, suggesting that factorized spatiotemporal attention effectively captures localized nearshore wave dynamics. The overall performance (smallest prediction spread across all wave period bins) is best for the model PtAttnCNN (TinyWaveNet) without physics regularization (WS: 0.9767, SI: 0.0924) and with strong physics regularization at $\lambda = 5.0$ (WS: 0.9811, SI: 0.0892).

The physics regularized PtAttnCNN ($\lambda = 5.0$) is recommended for operational use due to the low number of parameters (0.28 M), the shortest inference time (latency) in real-time (0.53 ms) and the best oceanographic skill scores. The advantages of the ROI optimization were found to be the decrease of the RMSE by 27%, and the absence of physically unrealistic predictions and the spurious spectral peaks. The temporal smoothness analysis also showed that the T_p estimation is consistent for the allowed number of consecutive frames in the video for the various oceanographic conditions (foam coverage and illumination). The framework has additional practically relevant attributes in addition to being correct. A good physics-informed warm start is demonstrated by a 86.93% reduction in the validation RMSE from 2.4012s at Epoch 1 to 0.3138s at Epoch 25 as the synthetic pre-training was used for Airy wave sequences. The moderate increase, but faster one was seen in the first two epochs (60.3%) signifying that there is a fast convergence at the initial stages of the training process. The lightweight LtViViT variant (2.36 M parameters) can be installed at the edge and the ROI detection module is uncoupled and does not need to be adjusted according to the camera angle. The characteristics of the proposed framework are well suited and cost-effective to be applied to any environment that has high data volume and/or complex logistics in the nearshore area as an alternative to the conventional in-situ sensor arrays and complex deployment of a radar system. The 13 scenarios being validated now cover some open-source videos from the sources mentioned in section 2.1.1 and also from South Atlantic coast of Namibia in a spatially representative area with a consistent long-period swell climate, in open beach, rocky headland and rocky breakwater areas. Future work will cover other world wave climates, e.g., wind-sea dominated (North Sea, Mediterranean) and other mixed swell regimes (Pacific), will be further validated and complementary parameters (significant wave height (Hs), wave direction, runup) will be included as will be hybrid transformer-recurrent architectures that could offer further latency reduction. The present analysis does not use a strictly held-out test set independent of the Phase 2 fine-tuning data since the small size of the expert-labeled Golden Set (13 scenes) did not allow a formal train-test split without significantly decreasing the amount of fine-tuning data. The Golden Set will be extended in the future to permit rigorous held-out evaluation.

In the end, it is an economically viable physically robust monitoring device for long-term coastal monitoring and it can be combined with passive video streams to provide support to the engineering, research and coastal management communities for erosion and accretion control, beach morphology prediction, and adaptation to climate change.

References

- Abdelhady, H.U., & Troy, C.D. (2023). A machine learning framework for extending wave height time series using historical wind records. *arXiv preprint arXiv:2309.14204*, ,
- Ahmed, T., Creedon, L., Gharbia, S.S. (2023). Low-cost sensors for monitoring coastal climate hazards: A systematic review and meta-analysis. *Sensors*, 23(3), 1717,

- Almar, R., Blenkinsopp, C., Almeida, L.P., Cienfuegos, R., Catalán, P.A. (2017). Wave runup video motion detection using the radon transform. *Coastal Engineering*, 130, 46–51,
- Bai, G., Wang, Z., Zhu, X., Feng, Y. (2022). Development of a 2-d deep learning regional wave field forecast model based on convolutional neural network and the application in south china sea. *Applied Ocean Research*, 118, 103012,
- Buscombe, D., Carini, R.J., Harrison, S.R., Chickadel, C.C., Warrick, J.A. (2020). Optical wave gauging using deep neural networks. *Coastal Engineering*, 155, 103593,
- den Bieman, J.P., de Ridder, M.P., van Gent, M.R. (2020). Deep learning video analysis as measurement technique in physical models. *Coastal engineering*, 158, 103689,
- Deo, I.K., & Jaiman, R.K. (2025). Predicting wave dynamics using deep learning with multistep integration inspired attention and physics-based loss decomposition. *arXiv preprint arXiv:2504.11433*, ,
- Egan, G. (n.d.). Wave statistic estimation from surfline video data using convnets.
- Fung, J. (2023). *Vision-based near-shore wave tracking and recognition for high elevation and aerial video cameras (python, opencv)*. <https://github.com/citrusvanilla/multiplewavetracking-py>. GitHub.
- Gomez, B., Giddings, S.N., Gallien, T. (2024). Infragravity wave oscillation forecasting in a shallow estuary. *Journal of Marine Science and Engineering*, 12(4), 672,
- James, S.C., Zhang, Y., O'Donncha, F. (2018). A machine learning framework to forecast wave conditions. *Coastal Engineering*, 137, 1–10,
- Jiao, L., Zhang, X., Liu, X., Liu, F., Yang, S., Ma, W., . . . others (2023). Transformer meets remote sensing video detection and tracking: A comprehensive survey. *IEEE Journal of Selected Topics in Applied Earth Observations and Remote Sensing*, 16, 1–45,

- Kaneko, T., Houtani, H., Wada, R., Inoue, T. (2025). Phase-resolved prediction of ocean wave field using video prediction. *Applied Ocean Research*, 154, 104358,
- Kinsela, M.A., Morris, B.D., Ingleton, T.C., Doyle, T.B., Sutherland, M.D., Doszpot, N.E., . . . Hanslow, D.J. (2024). Nearshore wave buoy data from southeastern australia for coastal research and management. *Scientific Data*, 11(1), 190,
- Lawal, Z.K., Yassin, H., Lai, D.T.C., Idris, A.C. (2025). Optimizing significant wave height forecasting through ensemble patch-tst and attention-enhanced recurrent models. *Environmental Modelling & Software*, 106803,
- Liu, Y., Li, R., Hu, W., Ren, P., Xu, C. (2025). Regional wave spectra prediction method based on deep learning. *Journal of Marine Science and Engineering*, 13(8), 1461,
- Mac Conamhna, O.A.P. (2020). *Extreme to phenomenal storm wave impacts on a steep rocky coast, north mayo, ireland: video data, image analysis, runup and flow velocity calculations for waves of storms fionn and gareth*. Zenodo. (Version 2)
- Naeini, S.S., & Snaiki, R. (2024). A physics-informed machine learning model for time-dependent wave runup prediction. *Ocean Engineering*, 295, 116986,
- Ouyang, L., Ling, F., Li, Y., Bai, L., Luo, J.-J. (2023). Wave forecast in the atlantic ocean using a double-stage convlstm network. *Atmospheric and Oceanic Science Letters*, 16(4), 100347,
- Ramesh, M., Nair, L.S., Anoop, T.R., Prakash, T.N. (2022). Nearshore wave analysis from coastal video monitoring techniques at high energy micro tidal beach under sunlight dominance conditions: a case study from valiathura beach in southwest coast of india. *Regional Studies in Marine Science*, 51, 102205,
- Rautenbach, C., Trenham, C., Benn, D., Hoeke, R., Bosserelle, C. (2022). Computing efficiency of xbeach hydro-and wave dynamics on graphics processing units (gpus). *Environmental Modelling & Software*, 157, 105532,

- Santos, D., Abreu, T., Silva, P.A., Santos, F., Baptista, P. (2022). Nearshore bathymetry retrieval from wave-based inversion for video imagery. *Remote Sensing*, 14(9), 2155,
- Sapiega, P., & Zalewska, T. (2024). Application of the high-resolution wave model for forecasting 1d sediment transport and beach inundation as a component of a short-term storm warning system. *Environmental Modelling & Software*, 179, 106089,
- Scardino, G., Scicchitano, G., Chirivì, M., Costa, P.J., Luparelli, A., Mastronuzzi, G. (2022). Convolutional neural network and optical flow for the assessment of wave and tide parameters from video analysis (leucotea): An innovative tool for coastal monitoring. *Remote Sensing*, 14(13), 2994,
- Shi, J., Su, T., Li, X., Wang, F., Cui, J., Liu, Z., Wang, J. (2023). A machine-learning approach based on attention mechanism for significant wave height forecasting. *Journal of Marine Science and Engineering*, 11(9), 1821,
- Sithara, S., Unni, A., Pramada, S. (2025). Machine learning approaches to predict significant wave height and assessment of model uncertainty. *Ocean Engineering*, 328, 121039,
- Smit, P.B., Egan, G., Houghton, I.A. (2024). Continuous peak period estimates from discrete surface-wave spectra. *Journal of Atmospheric and Oceanic Technology*, 41(6), 573–581,
- Turner, I.L., Leaman, C.K., Harley, M.D., Thran, M.C., David, D.R., Splinter, K.D., ... others (2024). A framework for national-scale coastal storm hazards early warning. *Coastal Engineering*, 192, 104571,
- Ursula von St Ange (2018a). *Cape point wavenet*. https://wavenet.csir.co.za/OnlineData/CapeTown/ct_m.htm. CSIR.
- Ursula von St Ange (2018b). *Development of an operational swan model for false bay: Virtual buoy system*. https://wavenet.csir.co.za/OnlineData/FalseBay/fb_m.htm. CSIR.
- Van der Westhuysen, A. (2012). Modeling nearshore wave processes. *Ecwmf workshop on ocean waves, european centre for medium-range weather forecasts, reading* (Vol. 1, pp. 50–61).

- Venkateswarlu, C., Gireesh, B., Ramesh, M., ArunKumar, S.V., Naidu, C.V., Nair, L.S., Sharma, R. (2025). Advancing nearshore wave monitoring: estimating parameters through video time stack imagery. *Ocean Dynamics*, 75(11), 93,
- Vieira, M., Soares, C.G., Guimarães, P.V., Bergamasco, F., Campos, R.M. (2025). Nearshore space-time ocean wave observation using low-cost video cameras. *Coastal Engineering*, 197, 104694,
- Vitousek, S., Buscombe, D., Vos, K., Barnard, P.L., Ritchie, A.C., Warrick, J.A. (2023). The future of coastal monitoring through satellite remote sensing. *Cambridge Prisms: Coastal Futures*, 1, e10,
- Wei, Z., & Davison, A. (2022). A convolutional neural network based model to predict nearshore waves and hydrodynamics. *Coastal Engineering*, 171, 104044,
- Xu, C., Li, R., Hu, W., Ren, P., Song, Y., Tian, H., ... Liu, Y. (2024). On the nearshore significant wave height inversion from video images based on deep learning. *Journal of Marine Science and Engineering*, 12(11), 2003,
- Yang, F., Wanik, D.W., Cerrai, D., Bhuiyan, M.A.E., Anagnostou, E.N. (2020). Quantifying uncertainty in machine learning-based power outage prediction model training: A tool for sustainable storm restoration. *Sustainability*, 12(4), 1525,
- Yu, T., & Wang, J. (2021). A spatiotemporal convolutional gated recurrent unit network for mean wave period field forecasting. *Journal of Marine Science and Engineering*, 9(4), 383,
- Zhang, C., & Li, M. (2023). Ocean wave information extraction from raw ocean video based on self-attention convlstm. *2023 international conference on new trends in computational intelligence (ntci)* (Vol. 1, pp. 375–380).
- Zhou, Z., Liu, J., Wu, R., Guo, A. (2025). Non-contact sensing methods for wave measurement: current research and challenge. *Intelligent Transportation Infrastructure*, 4, liaf003,